Unified Treatment of Thermodynamic and Optical Variability in a Simple Model of Unresolved Low Clouds

CHRISTOPHER A. JEFFERY AND PHILIP H. AUSTIN

Atmospheric Sciences Programme, University of British Columbia, Vancouver, British Columbia, Canada

(Manuscript received 16 May 2001, in final form 6 January 2003)

ABSTRACT

Comparative studies of global climate models have long shown a marked sensitivity to the parameterization of cloud properties. Early attempts to quantify this sensitivity were hampered by diagnostic schemes that were inherently biased toward the contemporary climate. Recently, prognostic cloud schemes based on an assumed statistical distribution of subgrid variability replaced the older diagnostic schemes in some models. Although the relationship between unresolved variability and mean cloud amount is known in principle, a corresponding relationship between ice-free low cloud thermodynamic and optical properties is lacking. The authors present a simple, analytically tractable statistical optical depth parameterization for boundary layer clouds that links mean reflectivity and emissivity to the underlying distribution of unresolved fluctuations in model thermodynamic variables. To characterize possible impacts of this parameterization on the radiative budget of a large-scale model, they apply it to a zonally averaged climatology, illustrating the importance of a coupled treatment of subgrid-scale condensation and optical variability. They derive analytic expressions for two response functions that characterize two potential low cloud feedback scenarios in a warming climate.

1. Introduction

Statistical cloud schemes have a long history that dates back to the pioneering work of Sommeria and Deardorff (1977) and Mellor (1977). Large-scale atmospheric models typically contain temperature, pressure, and total water (vapor + liquid) fields that evolve according to prescribed dynamical and thermodynamical equations. Traditionally these numerical models would assign, for each field, a single average value to an individual grid cell, thereby ignoring any variability within the cell. The relative importance of this neglected variability is, not surprisingly, scale dependent; for large-scale climate models with grid spacings of 250 km or greater the unresolved variability can be a substantial fraction of the mean value (Barker et al. 1996). Furthermore, the relative importance of subgrid variability is magnified manyfold by the presence of condensation, which is a small difference in two relatively large scalar quantities: the saturation vapor density, q_s, and the cell's total vapor (or water) density, q_t, prior to condensation. Early climate modelers were well aware that the use of ''all-or-nothing'' condensation schemes, whereby an individual grid cell is either completely clear or completely cloudy depending on the difference $q_t - q_s$, is a particularly acute problem (Manabe and Wetherald 1967).

The Sommeria–Deardorff–Mellor (SDM) statistical cloud scheme introduces a stochastic subgrid variable s that represents unresolved fluctuations in $q_s - q_t$ and is assumed to be normally distributed.[1] The variance of s, σ_s^2, in more sophisticated schemes can be diagnosed from a turbulence model (Ricard and Royer 1993) or from neighboring cells (Levkov et al. 1998; Cusack et al. 1999) but, in practice, is often taken as a prescribed fraction (Smith 1990) of q_s^2. A key assumption in the SDM scheme is that each grid cell is assumed to contain a complete ensemble of s from which the statistics of unresolved cloud are calculated, regardless of the size of the grid or the time step of the model. For example, the mean liquid water to some power p, $\overline{q_l^p}$, in the cloudy region of a cell is given by

$$\overline{q_l^p} = A_d^{-1} \int_{-\infty}^{q_t - q_s} a_L^p (q_t - q_s - s)^p P_s(s)\, ds$$

$$A_d = \int_{-\infty}^{q_t - q_s} P_s(s)\, ds, \tag{1}$$

where P_s is the probability distribution function (e.g., Gaussian) of s; the cloud density, A_d, is the fraction of

Corresponding author address: Christopher A. Jeffery, Los Alamos National Laboratory (NIS-2), P.O. Box 1663, Mail Stop D-436, Los Alamos, NM 87545.
E-mail: cjeffery@lanl.gov

[1] This notation differs from Mellor (1997), where s represents fluctuations in $q_t - q_s$.

grid cell occupied by cloud; and $a_L < 1$ is a parameter that accounts for the subadiabatic liquid water profiles typically observed in layer clouds. In what follows an overbar is reserved to represent an average over the cloudy fraction of a cell or column of cells, brackets $\langle \cdot \rangle$ represent a spatial average over the entire cell/column, and unresolved variability in each cell is assumed to be centered (i.e., have zero mean).

Statistical cloud schemes, in their current form, provide complete information about q_l but only limited information on cloud optical properties. This is because optical depth, τ, is a vertical integral of $q_l^p(z)$ from cloud base to cloud top and variability in q_l has nonzero spatial correlations produced by turbulence, that is, $\langle s(z_1)s(z_2)\rangle \neq 0$. Thus while the SDM scheme does provide grid-column-averaged optical depth $\langle\tau\rangle$, it does not provide $\overline{\tau}$ or higher-order moments without further assumption. In section 2 below we link thermodynamic and optical variability in the SDM scheme by first restricting s and hence P_s to be height independent in low clouds. At the same time, we consider a distribution of cloud-top height fluctuations (z'_{top}) that is distinct from a height-independent P_s. The resulting low-dimensional model is analytically tractable and requires only the specification of the z-independent joint z'_{top}-s distribution function to completely determine P_τ (Jeffery 2001).

Our approach extends the results of Considine et al. (1997), who showed that normally distributed cloud thickness fluctuations can produce distributions of integrated cloud liquid water path (LWP) (or, equivalently in their approximation, optical thickness) that qualitatively match Landsat satellite cloud observations for a range of cloud fractions. Our approach also builds upon the recent work of Wood and Taylor (2001), who linked s and P_τ but did not consider z'_{top}. Below we derive general forms for LWP(s, z'_{top}) and $\tau(s, z'_{\text{top}})$ in a layer with horizontally fluctuating cloud top and cloud base. We also adopt a radiation parameterization that incorporates P_τ into the calculation of longwave and shortwave fluxes.

Our analytic expressions for τ allow us to combine fluctuations in s and z'_{top} into a single subgrid variable s_*, and we examine the radiative response of the statistical cloud scheme to changes in the variance of s_* and hence the optical thickness distribution P_τ. We choose a form for P_{s*} suitable for large-scale models and similar to the triangle distribution of Smith (1990), adopting his choice for the temperature dependence of unresolved variability, $\sigma^2_{s*} \sim q_s^2(T)$. With this modeled coupling of P_τ to the surface temperature through q_s, we use the parameterization to investigate the change in net mean cloud reflectivity for a specified temperature change, given an idealized climatology.

Understanding the response of cloud-layer reflectivity to increasing temperature is complicated by the fact that the total reflectivity ($\langle R\rangle = A_c\overline{R}$) of a cloud layer is a nonlinear function of τ and cloud fraction A_c: the fraction of sky covered by cloud when viewed from below. Thus, for example, an increase in $\overline{q_l}$ (or $\overline{\tau}$) caused by increasing temperatures does not necessarily imply an increase in $\langle R\rangle$ if A_c decreases, producing an optically thicker cloud field with smaller cloud fraction. The coupling of our statistical approach to surface temperature allows us to investigate the combined ($\partial A_c/\partial T$, $\partial\overline{\tau}/\partial T$) response within an analytic framework.

The first theoretical study, and one of the only studies to date, that investigates the coupled (ΔA_c, $\Delta\overline{\tau}$) response of a cloud layer to increasing temperature (ΔT) while holding, alternatively, both A_c and $\overline{\tau}$ fixed is that by Temkin et al. (1975). Temkin et al. (1975) compared and contrasted the temperature sensitivity of A_c at fixed $\overline{\tau}$, $(\partial A_c/\partial T)_{\overline{\tau}}$, with the temperature sensitivity of $\overline{\tau}$ at fixed A_c, $(\partial\overline{\tau}/\partial T)_{A_c}$ in a simplified atmosphere with one cloud layer and constant surface relative humidity (RH). They found $(\partial A_c/\partial T)_{\overline{\tau}} > 0$ and $(\partial\overline{\tau}/\partial T)_{A_c} > 0$ using a nonstochastic model. These results indicate a negative low cloud feedback (LCF), where LCF is defined as the change in the net downward shortwave flux at the top of the cloud layer produced by a positive temperature change.

There have been numerous modeling and observational studies that suggest a range of values for the sign and magnitude of this cloud radiative response. For example, a negative low cloud (τ) feedback at high latitudes is also implied by the positive liquid water sensitivity $\partial q_l/\partial T$ found by Somerville and Remer (1984) in Russian aircraft measurements, assuming a negligible cloud thickness sensitivity. In contrast, Schneider et al. (1978) suggested that warming leads to increased convection and vertical q_t transport and a resulting atmosphere that is unable to increase q_t sufficiently to maintain constant RH. A relative drying of the lower atmosphere with warming implies that global cloud feedback may not be negative. Support for a positive cloud feedback is provided by the global climate model (GCM) study of Hansen et al. (1984), who found that clouds contribute a feedback of ≈1.5°C—nearly 1°C due to a reduction in low clouds—resulting in a net climate sensitivity double that found in an earlier study with fixed clouds (Manabe and Stouffer 1979). By 1990, all 19 of the GCMs compared by Cess et al. (1990) predicted a decrease in globally averaged A_c with increasing temperature, although the sign and magnitude of the net cloud feedback varies considerably from model to model. More recently, Tselioudis et al. (1993) analyzed global satellite observations of low cloud τ and found a generally negative optical depth sensitivity, $\partial\tau/\partial T$, (positive cloud feedback) which increases from the midlatitudes to the Tropics. A positive low/midlatitude low cloud (τ) feedback is also implied by the temperature dependence of satellite observations of liquid water path (Greenwald et al. 1995).

In this article we expand on the approach of Temkin et al. (1975) and calculate analytic response functions for our statistical treatment of low cloud optical vari-

ability. We find $(\partial A_c/\partial T)_{\overline{\tau}} < 0$ in contradistinction with Temkin et al. (1975). This result links the observational evidence of a largely negative $\overline{\tau}$ sensitivity (Tselioudis et al. 1993; Greenwald et al. 1995) with GCM simulations that predict a negative A_c response (Cess et al. 1990) as we discuss in section 4.

The article is organized as follows. In section 2 we derive our statistical model and compare the predictions of the model with satellite data taken from Barker et al. (1996). The behavior of our scheme is analyzed in section 3 using an idealized zonally averaged climatology and in section 4 we present A_c–$\overline{\tau}$–T response functions. Section 5 contains a summary.

2. Model description

Our model of boundary layer cloud optical variability is based on two assumptions: 1) horizontal subgrid variability in the boundary layer of large-scale models exceeds vertical variability; and 2) cloud liquid water increases linearly with height above cloud base, that is, $q_s(z) = q_0 - \Gamma_w z$ where $\Gamma_w > 0$. Assumption 1 is accurate for large-scale temperature and moisture fluctuations because the horizontal length of a grid cell in a climate model is much greater than the boundary layer height. However, it does not hold near cloud top where the vertical dependence of s at the cloud boundary is complex. We overcome this deficiency by introducing a distribution of unresolved cloud-top height fluctuations, $P_{z'_{\text{top}}}$, that is distinct from a z-independent P_s, although s and z'_{top} may be correlated. Our second assumption is well supported both numerically and experimentally in the literature.

Given assumptions 1 and 2 we are now in a position to calculate the optical statistics of low clouds. For clarity and brevity, we first introduce the notation. The variable dependence (x) labels unresolved horizontal variability, whereas (z) indicates a vertical dependence, which, by assumption 1 is nonstochastic; that is, subgrid vertical fluctuations are assumed negligible. Furthermore, (x) represents unresolved variability in a single cell whereas (z) is a continuous dependence that may extend through a column of cells.

a. Linking P_s and $P_{z'_{top}}$ to P_τ

Consider the integral of $q_l^p(z, x)$ from cloud base $z_{\text{bot}}(x)$ to cloud top $z_{\text{top}}(x) = z_{\text{top}} + z'_{\text{top}}(x)$:

$$\int_{z_{\text{bot}}(x)}^{z_{\text{top}}(x)} q_l^p(z, x)\, dz = \frac{a_L^p \Gamma_w^{-1}}{p+1}\{q_t + \Gamma_w z_{\text{top}} - q_0 - s_*(x)\}_H^{p+1}, \quad (2)$$

where

$$s_*(x) = s(x) - \Gamma_w z'_{\text{top}}(x), \quad (3)$$

$\{A\}_H : \{A < 0\}_H = 0$, $\{A \geq 0\}_H = A$ is a Heaviside bracket and we have used $z_{\text{bot}} = \Gamma_w^{-1}(q_0 - q_t + s)$ from assumption 2. The key feature of Eqs. (2) and (3) is that fluctuations in z_{bot} are defined by inverting $q_l(z_{\text{bot}}, s) = 0$, whereas the unresolved cloud-top height fluctuations z'_{top} are absorbed into the new subgrid variability s_*. Thus our distribution $P_{z'_{\text{top}}}$ can, in principle, be combined with P_s to give P_{s*}. This is advantageous because unresolved variability of q_t, q_s, and z_{top} is contained in the single parameter s_* and P_{s*} is z independent. In analogy with the SDM scheme we assume that s_* is centered and P_{s*} is known. The rhs of Eq. (2) should not be confused with $q_l^{p+1}(z_{\text{top}}, x)a_L^{-1}\Gamma_w^{-1}/(p+1)$ from Eq. (1) since the statistics of s_* generally differ from the statistics of s.

Formulation of the shortwave and longwave optical depths follows from Eq. (2) given the appropriate functional relation $\tau \sim \int \text{func}(q_l, \ldots)\, dz$. At this point, it is convenient to introduce the cloud thickness $h(x) = z_{\text{top}}(x) - z_{\text{bot}}(x)$ so that Eq. (2) is simply

$$\int_{z_{\text{bot}}(x)}^{z_{\text{top}}(x)} q_l^p(z, x)\, dz = \frac{(a_L\Gamma_w)^p}{p+1} h^{p+1}(x). \quad (4)$$

The longwave optical depth, because it depends primarily on the LWP, is strictly given by the "h^2 model":

$$\tau(x) \sim h^2(x) \sim \frac{a_L}{2\Gamma_w}\{q_t + \Gamma_w z_{\text{top}} - q_0 - s_*(x)\}_H^2. \quad (5)$$

In contrast, a number of different formulations exist for the shortwave optical depth. For example, writing τ in terms of LWP and a constant effective radius (r_{eff}) recovers the h^2 model. In layer clouds a better approach due to Pontikis (1993) is to assume proportionality of the effective and volume-averaged radius, $r_{\text{eff}} \sim q_l^{1/3}$, giving $p = 2/3$ and a 5/3 dependence of τ on h [Pontikis 1993, (Eq. 5)]. Thus we have the "$h^{5/3}$ model" for shortwave optical depth:

$$\tau(x) \sim \frac{3a_L^{2/3}}{5\Gamma_w}\{q_t + \Gamma_w z_{\text{top}} - q_0 - s_*(x)\}_H^{5/3}. \quad (6)$$

Note that inherent in Eq. (6) is the approximation that the cloud droplet concentration, N, is independent of s_*, an approximation that is likely accurate if the majority of low clouds in a grid cell are non- or weakly precipitating.

The constant of proportionality in Eq. (6) goes as $N^{1/3}$ (Pontikis 1993; see also appendix C). In what follows we ignore the effect of unresolved fluctuations in N on the statistics of τ. This approximation is unlikely to be valid near large sources of N, for example, major industrial cities, but is justifiable elsewhere because the 5/3 moment of q_l acts to magnify fluctuations while the 1/3 moment of N acts to damp fluctuations. This behavior is illustrated with the following example. Consider the dependence of $\langle(Y_0 + Y')^\alpha\rangle$ on mean value Y_0 and the variance of Y',

σ_Y^2, where Y' is normally distributed. Writing $\langle (Y_0 + Y')^\alpha \rangle \sim Y_0^{\alpha-\beta}\sigma_Y^\beta$ we find ($\alpha = 1/3$, $\beta \approx -0.15$) and ($\alpha = 5/3$, $\beta \approx 0.5$) for the range $\sigma_Y \leq Y_0 \leq 2\sigma_Y$. Hence, increasing σ_{q_l} at fixed $q_{l,0}$ acts to increase $\langle (q_{l,0} + q_l')^{5/3} \rangle$ as expected but a similar increase in σ_N decreases $\langle (N_0 + N')^{1/3} \rangle$ because of the damping effect of the 1/3 exponent. This result suggests that the normalized variance of N would have to be 3 to 4 times larger than the normalized variance of q_l for unresolved droplet number fluctuations to have a comparable effect on the statistics of τ.

The moments of τ can be calculated from P_{s*} in analogy with P_s in Eq. (1) while A_c is given by

$$A_c = \int_{-\infty}^{q_t - q_s(z_{\text{top}})} P_{s_*}(s_*)\, ds_*. \tag{7}$$

Intuitively, we might expect the maximum cloud overlap assumption, $A_c = \max(A_d) = A_d(z_{\text{top}})$, to hold for a model of cloud variability that ignores vertical variations in s. However, comparing Eqs. (1) and (7) we find that it does not hold generally since A_c is calculated from P_{s*} and not P_s. The failure of the maximum cloud overlap assumption is due to the independence of z'_{top} and s in our approach. Note that the usual cell averaged quantities, For example, $\overline{q_l}(z)$, are independent of z'_{top} and should be calculated with P_s.

b. Approximations for P_s and P_{s*}

Knowledge of both P_s and $P_{z'_{\text{top}}}$, and hence P_{s*}, is limited. Cloud ensemble (Xu and Randall 1996), large eddy simulations (LES; Cuijpers and Bechtold 1995), and observational studies (Larson et al. 2001) provide support for a Gaussian P_s. Comparatively less is known about $P_{z'_{\text{top}}}$. Ground-based (Boers et al. 1988; Albrecht et al. 1990) and space-based (Strawbridge and Hoff 1996; Loeb et al. 1998) retrievals of z'_{top} suggest a standard deviation of 50–100 m for marine stratus over typical GCM length ($\approx$100 km) and time ($\approx$2 h) scales. A comprehensive analysis of the shape of $P_{z'_{\text{top}}}$ is currently lacking.

Observational (Klein and Hartmann 1993; Oreopoulos and Davies 1993; Norris and Leovy 1994; Klein et al. 1995; Bony et al. 1997) studies of the marine boundary layer over relatively long timescales suggest that s is largely a function of boundary layer temperature, T, while z_{top} is largely controlled by the jump in potential temperature ($\Delta\theta$) at the top of the boundary layer. Defining an interfacial Richardson number (Deardorff 1981)

$$\text{Ri} \equiv (g/T) z_{\text{top}} \Delta\theta / w_*^2$$

where w_* is Deardorff (1974)'s convective velocity scale, Moeng et al. (1999) estimate the standard deviation of z'_{top} as

$$\sigma_{z'_{\text{top}}}/z_{\text{top}} \approx 0.6\ \text{Ri}^{-1}$$

from LESs of a cloud-topped boundary layer. Thus we find that the variance of s_*

$$\sigma_{s*}^2 \sim \left(\frac{\partial q_0}{\partial T}\sigma_T\right)^2 + \{\Gamma_w z_{\text{top}}\, \text{Ri}^{-1}\}^2. \tag{8}$$

As mentioned previously $\sigma_s(z)$ is usually assumed to be proportional to $q_s(z)$, that is, σ_T = constant. Assuming that z_{top} and Ri are T independent as well permits a particularly simple form for the temperature dependence of P_{s*}.

Recent observational studies (Norris 1998a,b; Bajuk and Leovy 1998; Chen et al. 2000) have indicated the importance of cloud type in the analysis of cloud properties; in principle the ratio σ_{s*}/σ_s could be parameterized as a function of cloud type diagnosed from various stability and potential energy considerations. On the other hand, in consideration of the poor boundary layer vertical resolution of typical GCMs and in the absence of knowledge of σ_{s*}/σ_s, we follow current GCM parameterizations and assume $\sigma_{s*} \sim \sigma_s \sim q_s$ in section 3. Note that $\sigma_{z_{\text{top}}}$ is coupled to q_s through Γ_w in Eq. (3). Since s_* is z independent by definition in our scheme we will use $q_s(z)$ at the surface [i.e., $q_0(T)$] to evaluate the temperature dependence of σ_{s*} in section 3.

c. Radiation

Currently, most GCMs lack the methodology to include unresolved variability in the calculation of cloud reflectivity (R) or emissivity (ϵ). This deficiency may have important implications for the prediction of global cloud feedback discussed above. Through the use of a statistical cloud scheme [e.g., SDM, Eq. (1)], many modern GCMs couple changes in cloud properties [e.g., (ΔA_c, $\Delta\overline{\tau}$)] in a changing climate to the distribution of the subgrid variability s. But they also use the plane-parallel homogeneous (PPH) assumption $\overline{R_{\text{pph}}} = R(\overline{\tau})$, which decouples the optical properties R and ϵ from the underlying thermodynamic cloud variability. The convexity of the functions relating R and ϵ to τ ensures that the optical bias incurred from the PPH assumption is positive, that is, $\overline{R}$ and $\overline{\epsilon}$ are overestimated. To reduce this bias many current GCMs use an effective optical depth $\tau_{\text{eff}} = \chi\overline{\tau}$ where $\chi \approx 0.7$ to calculate $\overline{R_{\text{pph}}}$ (Cahalan et al. 1994). Although χ may be tuned in a particular GCM to reproduce the measured radiative stream, this approach is ad hoc in nature and becomes increasingly inaccurate as the climate departs from its present state. Below we present a unified treatment of the thermodynamic and optical variability of boundary layer clouds based on the SDM scheme.

The utility of Eqs. (5) and (6) is not in the calculation of τ directly but, rather, in providing a methodology to include subgrid variability in the reflectivity and emissivity. We do this by calculating $P_\tau(\tau)$ from P_{s*} using the equations above and a change of variable; then by definition

$$\overline{X} = \int X(\tau) P_\tau(\tau)\, d\tau, \tag{9}$$

where $X = R$ or ϵ and P_τ is the distribution of τ in the cloudy part of the column. This approach is discussed in Considine et al. (1997) and Pincus and Klein (2000), albeit not in the context of a generalized framework of unresolved variability. Unfortunately, the analytic expressions for R and ϵ are sufficiently unwidely to prevent an analytic evaluation of Eq. (9).

Another approach, pioneered by Barker (1996), is to assume an analytically friendly form for P_τ that is both sufficiently general to approximate P_τ over a wide range of conditions and that allows a closed-form expression for $\overline{X}$. Barker et al. (1996) analyzed satellite data of marine low clouds and found that a generalized γ distribution, $P_\gamma(\tau)$, closely approximates the observed distribution and allows Eq. (9) to be integrated analytically.

The last step in our treatment of unresolved optical variability is to relate P_γ to Eqs. (5) or (6) and P_{s*}. The shape of P_γ is controlled by the parameter $\nu = \overline{\tau}^2/\sigma_\tau^2$, which is a measure of the width of the distribution relative to its mean. Barker (1996), who introduced $P_\gamma(\nu, \tau)$, did not relate ν, and in particular σ_τ^2, to the unresolved thermodynamic variability s. Using the framework we have presented thus far, we calculate $\overline{\tau}$ and $\overline{\tau^2}$ (and thus ν) using Eqs. (5) or (6), and P_{s*} substituted for P_s in Eq. (1). Analytic expressions for $\overline{R}(\nu, \overline{\tau})$ and $\overline{\epsilon}(\nu, \overline{\tau})$ used in our analysis in section 3 are given in Barker (1996) and Barker and Wielicki (1997), respectively.

d. Comparison with Landsat data

Our scheme provides a one-to-one relationship between ν and A_c for a given P_{s*} that can be tested against the Landsat satellite data compiled by Barker et al. (1996). To make such a comparison we need to specify the distribution P_{s*}. Considine et al. (1997) assumed a normally distributed h—equivalent to a normally distributed s_* in our formulation—and found that the A_c dependence of the LWP distribution predicted by the h^2 model is consistent with Landsat data. Using the (Gaussian) Considine model, Wood and Taylor (2001) derived an approximate relationship between $\overline{\text{LWP}}$ and σ_{LWP} for large A_c and verified this relationship using First ISCCP (International Satellite Cloud Climatology) Regional Experiment data. In appendix A we present exact analytic results for $\overline{\text{LWP}}$ and $\overline{\text{LWP}^2}$, and hence σ_{LWP}, that are valid for all A_c.

A potential disadvantage in assuming a normally distributed s_* is that closed-form expressions for noninteger moments, for example, the $h^{5/3}$ model, are not available. The triangle distribution first used by Smith (1990) is a computationally efficient surrogate for the Gaussian distribution that is analytically tractable, but it does not accurately mimic a Gaussian at small A_c. We therefore introduce a modified triangle distribution (appendix B) that is similar to Smith's scheme (or a Gaussian) at large A_c but better reproduces Gaussian behavior at small A_c. In particular, our distribution gives $P_{s*} > 0$ for a wider range of s_*, $|s_*| < (35/3)^{1/2}\sigma_{s*}$, than Smith (1990)'s triangle, $|s_*| < (6)^{1/2}\sigma_{s*}$. An expression for the arbitrary moment $\overline{\tau^\lambda}$ is given in appendix B.

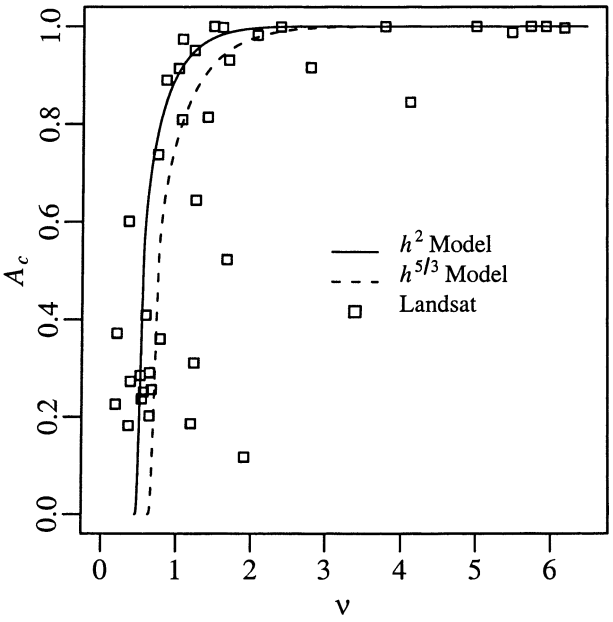

FIG. 1. Plot of A_c vs ν for the h^2 and $h^{5/3}$ models calculated using Eqs. (5)–(7), and P_s from appendix B. Landsat data in the range $\nu \leq 6.5$ from Table 2* of Barker et al. (1996) is also shown for comparison.

A comparison of A_c versus ν is shown in Fig. 1 for the h^2 and $h^{5/3}$ models calculated using Eqs. (5)–(7), and our new triangle distribution (appendix B). Also shown is a subset, $\nu \in (0, 6.5)$, of the Landsat data tabulated in Table 2 of Barker et al. (1996). Agreement between the data and both theoretical models is good despite uncertainties in the retrieval of A_c from the satellite scenes (Barker et al. 1996). It should be noted that $\nu \in (6.5, 12)$ has a significant impact on the calculation of $\overline{R}$ and $\overline{\epsilon}$ and is in close agreement with the model, while the selected data shown in Fig. 1 emphasize the region $\nu \in (0.5, 3)$. However, it is encouraging that the asymptotic behavior near $\nu = 0.5$ predicted by our model is consistent with the data.

3. Low cloud radiative feedback using a simple climatology

As a demonstration of the behavior of our statistical cloud scheme, we now consider the coupling of unresolved variability and cloud feedback in the model of section 2 using a zonally averaged climatology. We consider only the response of low clouds and we specify a fixed (2°C) surface temperature perturbation. Since the

prognosed cloud changes do not feed back into the temperature perturbation our model experiments are an open-loop study. While our model neglects the meridional structure of cloud amount caused by atmospheric dynamics, for example, the storm tracks, and meridional variations in surface properties or σ_s (Rotstayn 1997), we incorporate what we consider to be the major latitudinal dependencies: solar zenith angle, saturation vapor density, and surface albedo. We further assume that droplet number concentration is T independent.

In this section and in the spirit of Temkin et al. (1975), we consider three different responses of a zonally averaged climatology to a fixed global increase in temperature. In our ''observationally constrained $\overline{\tau}$'' response (CT_{obs}) model mean optical depth decreases with increasing T according to a parameterization (appendix D) of the satellite observations of Tselioudis et al. (1993). By specifying the sensitivity $\Delta\overline{\tau}$ and assuming $\sigma_{s*} \sim q_s(z = 0, T) = q_0(T)$ we then predict ΔA_c using Eqs. (6) and (7). Following Temkin et al. (1975) we also consider (i) a ''constrained $\overline{\tau}$'' response (CT) model with constant $\overline{\tau}$, and (ii) a ''constrained A_c'' response (CA) model where A_c remains constant and we determine $\Delta\overline{\tau}$ from our unified scheme. In these calculations we do not determine q_t and z_{top} independently; for example, the negative optical depth sensitivity observed by Tselioudis et al. (1993) could result from a decrease in z_{top} despite increasing specific humidity (Tselioudis et al. 1998). Here our CT_{obs}, CT, and CA model experiments represent three possible scenarios of the climate's response to increasing temperatures that may have very complex dynamical origins and spatial structure. We do not make any claims that either CT_{obs}, CT, or CA is a ''most probable'' low cloud response. Rather, we hope to use these experiments to gain some insight into the relationship between low cloud radiative feedback and the coupled (ΔA_c, $\Delta\overline{\tau}$) response.

First consider our base-state climatology. Our zonally averaged model extends over latitudes $\phi = -60°$S to 60°N where our ''grid cells'' encompass one latitudinal band. We assume that our new triangle distribution (appendix B) defines the shape of the distribution P_{s*} that represents meridional fluctuations in ''subgrid'' variability, and that this form is independent of ϕ and T. Our base-state climatology is constructed from the $A_c(\phi)$ measurements of Warren et al. (1988) [See Ramaswamy and Chen (1993) and Kogan et al. (1997) for a similar approach.] Mean optical depth $\overline{\tau}(\phi) \in (3.5,6.2)$ is estimated from the satellite measurements presented in Hatzianastassiou and Vardavas (1999). Parameter values are given in appendix C. By specifying A_c, $\overline{\tau}$, $T(\phi)$, and $q_s(T)$, we solve for the two unknowns σ_{s*} and $q_t + \Gamma_w z_{top}$. We use the more accurate $h^{5/3}$ model for $\tau(h^2$ model for longwave τ).

The mean reflectivity and emissivity of our base-state climatology, averaged over the diurnal cycle at equinox, is shown in Fig. 2 along with the corresponding values predicted by the plane-parallel homogeneous approximation used by GCMs. The well-documented plane-parallel albedo (reflectivity) bias (Cahalan et al. 1994) of $\overline{R_{pph}}$, roughly 0.06 in our model, is visible in the lower half of the figure, but it is overshadowed by the much larger bias of $\overline{\epsilon_{pph}}$ that averages near 0.3. Early studies of τ feedback (Temkin et al. 1975; Somerville and Remer 1984) assumed that longwave optical properties of clouds are saturated ($\overline{\epsilon} = 1 \approx \overline{\epsilon_{pph}}$) and as a result, changes in τ only affect the cloud's shortwave properties. Although, as shown in Fig. 2, $\overline{\epsilon}$ is not saturated at global scales in our model, assumptions concerning the behavior of $\overline{\epsilon}$ are not significant for low cloud radiative forcing calculations since the longwave forcing is very small. Note that the PPH biases calculated using zonally averaged values of $\overline{\tau}$ and A_c are larger than the biases associated with a typical, partially cloudy GCM grid cell for which the cloud fraction tends to exceed that of our zonal climatology. Figure 2 reiterates that a coupled treatment of thermodynamic and optical variability can substantially impact the predicted values of low cloud $\overline{R}$ and $\overline{\epsilon}$ in a GCM cloud parameterization.

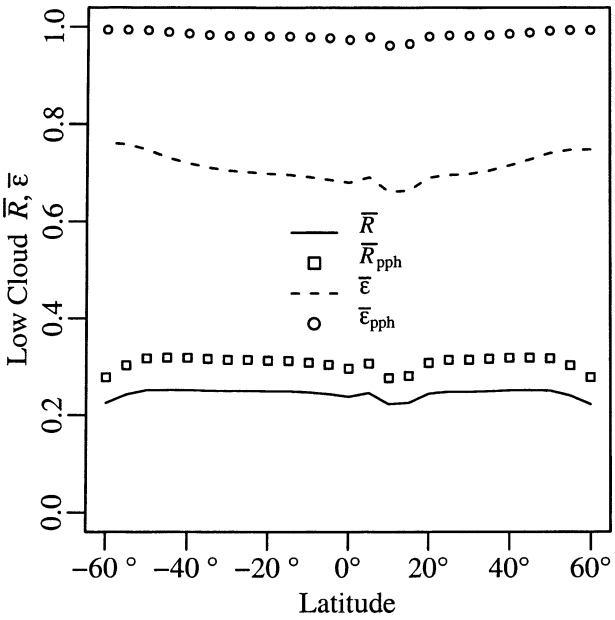

FIG. 2. Comparison of $\overline{R}$ and $\overline{\epsilon}$ with PPH values $\overline{R_{pph}} = R(\overline{\tau})$ and $\overline{\epsilon_{pph}} = \epsilon(\overline{\tau})$. The convexity of R and ϵ ensures that the PPH approximation overestimates $\overline{R}$ and $\overline{\epsilon}$. Shortwave $\overline{\tau}$ [Eq. (6)], longwave $\overline{\tau}$ [Eq. (5)], and A_c [Eq. (7)] are all calculated using P_s from appendix B. Expressions for $\overline{R}$ and $\overline{\epsilon}$ are from Barker (1996) and Barker and Wielicki (1997), respectively. Reflectivities are diurnally averaged at equinox. See appendix C for parameter values.

We now turn our attention to the modeled response of low cloud properties to warming. Consider a $\Delta T = 2$°C globally uniform warming where the sensitivity $\overline{\tau}(T + \Delta T)$ is prescribed to be (mostly) negative in the CT_{obs} model, $\overline{\tau}(T + \Delta T) = \overline{\tau}(T)$ constrains the CT model and $A_c(T) = A_c(T + \Delta T)$ constrains the CA model. The low cloud feedback predicted by the CT_{obs}, CT, and CA models is shown in Fig. 3. As before we define LCF as the change

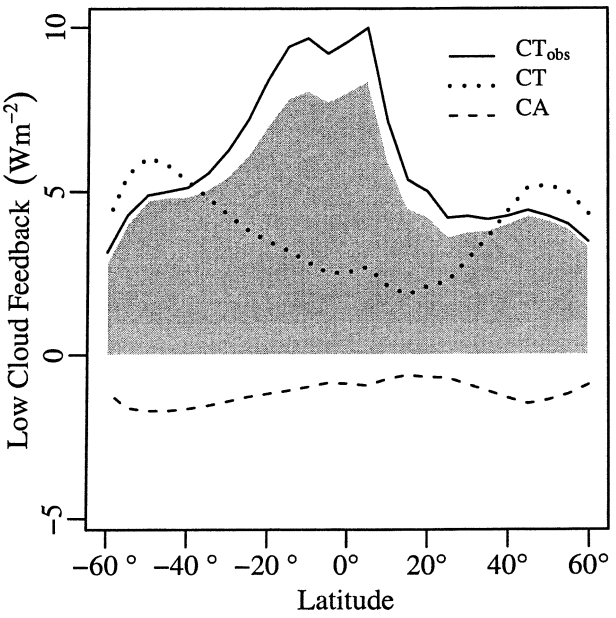

FIG. 3. Plot showing LCF predicted by the CT_{obs}, CT, and CA models for a uniform 2°C increase in global mean temperature. Since low clouds cool the earth by reflecting solar radiation, less low cloud (CT_{obs} and CT) enhances warming (positive cloud feedback) while more low cloud (CA) buffers the warming (negative cloud feedback). The shaded region indicates the dominant contribution of the A_c response to the overall CT_{obs} feedback. See appendix D for calculation details.

in the net (positive downward) radiative flux at the top of the boundary layer. The calculations employ the diurnally averaged equinox $\overline{R}$ and $\overline{\epsilon}$ predicted by our unified approach and the approximation $\sigma_{s*}(T + \Delta T) \approx \lambda_1 q_0(T + \Delta T)$ where $\lambda_1 = \sigma_{s*}(T)/q_0(T)$. The figure illustrates that the CT_{obs} and CT feedbacks are positive and considerably larger in magnitude than the negative LCF ($\overline{\tau}$ feedback) of the CA model. Moreover, in the tropical regime $-20° \leq \phi \leq 20°$ the CT_{obs} cloud feedback—a mixture of negative A_c and $\overline{\tau}$ response—is as much as 3.5 times as large as the CT cloud feedback. The CT_{obs} and CT cloud feedbacks are also generally larger than the $2 \times CO_2$ forcing of $\approx$4 W m^{-2}. However, it is important to emphasize that LCF is not a top-of-the-atmosphere feedback. In particular, modulation of the longwave stream through changes in high cloud properties could enhance or buffer the net cloud feedback.

Further analysis (not shown) reveals that LCF is relatively insensitive to the treatment of unresolved optical variability; LCF computed using plane-parallel homogeneous optical properties overestimates the CT_{obs} cloud feedback by 15% and the CA feedback by 35% compared to the predicted values shown in Fig. 3. Thus, clearly it is the constrained response of our modeled climate, that is, CT_{obs} vs. CT vs. CA, and not the parameterization of optical variability that determines LCF to first order. This finding is consistent with the GCM sensitivity study of Rotstayn (1999), among others.

To further explore the CT_{obs} cloud feedback, the relative contribution of the A_c response has been shaded in Fig. 3. The shading reveals that the total CT_{obs} feedback is dominated by the negative A_c response, even in the Tropics where the change in $\overline{\tau}$ is largest (Tselioudis et al. 1993). This behavior is in qualitative agreement with the recent $2 \times CO_2$ GCM experiments of Tselioudis et al. (1998, their Fig. 14), which show a relatively small $\overline{\tau}$ feedback of $\approx$0.2°C compared to the $\approx$1.5°C A_c feedback reported with an older version of the same GCM (Hansen et al. 1984). The dominance of A_c over $\overline{\tau}$ feedback is also in agreement with the regional observational studies of Oreopoulos and Davies (1993) (Tropics) and Bony et al. (1997) (subtropics), which imply that the negative A_c response may make a larger contribution to shortwave low cloud feedback than the negative $\overline{\tau}$ response. Several other observational studies (Klein and Hartmann 1993; Norris and Leovy 1994; Klein et al. 1995) also provide support for a negative A_c response.

4. A_c–$\overline{\tau}$–T response functions

Observational studies of cloud fraction sensitivity ($\partial A_c/\partial T$) and optical depth sensitivity ($\partial\overline{\tau}/\partial T$) are often used to provide insight into cloud feedback. As pointed out by Arking (1991), the information provided by these studies is limited because it is not known which parameters are held fixed and which are allowed to vary. In this section we present analytic response functions, $(\partial A_c/\partial T)_{\overline{\tau}}$ and $(\partial\overline{\tau}/\partial T)_{A_c}$, for our subgrid-scale cloud parameterization that do not suffer from this deficiency. Our use of the terminology ''response function'' is an analogy to response functions in the theory of thermodynamics, for example, specific heat and adiabatic compressibility of an ideal gas. We compare our results with the earlier study by Temkin et al. (1975), discussed in section 1, and assess the impact of coarse vertical resolution on a discrete numerical evaluation of these functions.

Combining Eqs. (6) and (7), $\sigma_{s*} \approx \lambda_1 q_s$, $\Gamma_w \approx \lambda_2 q_s$ and Smith's triangle distribution for subgrid variability (Smith 1990), we derive

$$\left(\frac{\partial \ln A_c}{\partial T}\right)_{\overline{\tau},\lambda} = -\frac{4}{5} q_s^{-1} \frac{\partial q_s}{\partial T} = -\frac{4}{5}\frac{L_v}{R_v T^2} \tag{10}$$

$$\left(\frac{\partial \ln \overline{\tau}}{\partial T}\right)_{A_c,\lambda} = \frac{2}{3}\frac{L_v}{R_v T^2}, \tag{11}$$

valid for $A_c \leq 0.5$, where $\lambda = \{\lambda_1, \lambda_2\}$, L_v is the latent heat of vaporization, R_v is the gas constant for water vapor, and recall that q_s must be evaluated at some fixed height (e.g., at the surface) since σ_{s*} and Γ_w are z independent by definition. For $A_c > 0.5$, Eq. (11) remains valid but for Eq. (10) $(\partial \ln A_c/\partial T)_{\overline{\tau},\lambda}$ decays monotonically to zero as $A_c \to 1$. The disappearance of the A_c response as $A_c \to 1$ reflects the increasing independence of A_c to small changes in σ_{s*} in the limit of vanishing unresolved variability. Overall the more general result $(\partial \ln A_c/\partial T)_{\overline{\tau},\lambda} \leq 0$ and $(\partial \ln\overline{\tau}/\partial T)_{A_c,\lambda} \geq 0$ is valid for all A_c.

We can interpret Eqs. (10) and (11) as representing two potential low cloud shortwave feedback scenarios in a warming climate demarcated by $\partial\overline{\tau}/\partial T = 0$ and $\partial A_c/\partial T = 0$, respectively. Let $F < 0$ be the net (positive downward) shortwave radiative flux reflected by the (unforced) low clouds and $\Delta T > 0$ be the thermal forcing. Consider the small τ approximation $F \sim A_c\overline{\tau}$. Then Eq. (10) implies LCF $= -(4/5)F\Delta T/T_*$, a positive cloud feedback, while for Eq. (11), LCF $= (2/3)F\Delta T/T_*$, a negative cloud feedback, where $T_* = R_v T^2/L_v$.

Although we make no claims regarding the likelihood of the two scenarios described by Eqs. (10) and (11), the difference in sign of Eqs. (10) and (11) leads to a nontrivial asymmetry between the $(A_c, \overline{\tau})$ response and LCF. Using Eq. (10) we find that $(\partial\overline{\tau}/\partial T)_\lambda \leq 0$ is a sufficient condition for a positive LCF while Eq. (11) implies that $(\partial A_c/\partial T)_\lambda \geq 0$ is a sufficient condition for a negative LCF. These relations follow from the positive coupling between A_c and $\overline{\tau}$, that is, $(\partial\overline{\tau}/\partial A_c)_{T,\lambda} > 0$. On the other hand, $(\partial\overline{\tau}/\partial T)_\lambda > 0$ and $(\partial A_c/\partial T)_\lambda < 0$ do not uniquely specify the sign of the LCF. Thus our statistical approach links the observational evidence of a largely negative $\overline{\tau}$ sensitivity (Tselioudis et al. 1993; Greenwald et al. 1995; Bony et al. 1997) with GCM simulations (Hansen et al. 1984; Wetherald and Manabe 1986; Colman and McAvaney 1997; Yao and Del Genio 1999) that predict a negative A_c sensitivity and a positive LCF. It is important to note that although these GCMs do not explicitly use a statistical cloud scheme, their RH-based grid-cell parameterizations for A_d (and hence A_c) are formally analogous to Eq. (1) for A_d with $\sigma_s^2 \sim q_s^2(T)$.

It is interesting to compare our negative A_c response function, Eq. (10), with the result $(\partial A_c/\partial T)_{\overline{\tau}} > 0$ derived by Temkin et al. (1975) using a nonstochastic model. In the Temkin et al. (1975) model, the increase in available liquid water with increasing temperature (recall RH is fixed) is placed in a formerly clear column that thereby increases A_c. In contrast, in our statistical approach the cloud thickness decreases in the face of increasing Γ_w resulting in a negative A_c sensitivity.

We extend Eq. (11) to another useful form through the approximation $(\partial \ln\overline{\tau}/\partial T)_{A_c,\lambda} \approx 2(\partial \ln\overline{R}/\partial T)_{A_c,\lambda}$ valid for $\overline{\tau} = O(5)$, giving

$$\left(\frac{\partial \ln\overline{R}}{\partial T}\right)_{A_c,\lambda} = \frac{1}{3}\frac{L_v}{R_v T^2}. \tag{12}$$

Since LCF is relatively insensitive to changes in $\overline{\epsilon}$ we can combine Eqs. (10) and (12):

$$\frac{|(\mathrm{LCF})_{\overline{\tau},\lambda}|}{|(\mathrm{LCF})_{A_c,\lambda}|} = 2.4,$$

which illustrates that, in general, A_c feedback dominates the $\overline{\tau}$ feedback in this model. The approximate 1:2.4 LCF ratio is illustrated by the CT and CA models in Fig. 3.

We can also use our response functions to quantify the effect of low model vertical resolution on LCF. The representation of low clouds in GCMs is poor; in particular GCMs tend to underpredict persistent marine stratocumulus cloud sheets in eastern ocean subsidence regions (Browning 1994; Bushell and Martin 1999). Typically GCMs have only four to six model levels in the boundary layer (BL) and the vertical resolution of these levels usually decreases with height. As a result, the top model level in the BL will dominate the discrete integration of q_l^p [Eq. (2)] and hence τ. In this low resolution limit the $h^{5/3}$ model for shortwave optical depth [Eq. (6)] becomes

$$\tau(x) \sim \{q_t + \Gamma_w z_{\mathrm{top}} - q_0 - s_*(x)\}^{2/3}\Delta z,$$

where Δz is the thickness of the model level centered at z_{top}. Computing the low vertical resolution response functions we find that the $\overline{\tau}$ response [Eq. (11)] remains unchanged while the A_c response becomes

$$\left(\frac{\partial \ln A_c}{\partial T}\right)_{\overline{\tau},\lambda_1,\Delta z} = -2\frac{L_v}{R_v T^2}, \tag{13}$$

independent of Γ_w. A comparison of Eqs. (10) and (13) reveals that RH-based implementations of statistical cloud schemes in low vertical resolution GCMs tend to overestimate the unresolved low cloud A_c response by a factor of 2.5 for $A_c \leq 0.5$, compared to the same statistical cloud scheme run at higher vertical resolution.

5. Summary

Understanding the complex interaction of clouds, radiation, and climate is a formidable challenge; the sign and magnitude of the global cloud feedback remains a question of concern and debate. In this study we focus on one facet of the cloud–climate interaction problem, namely, the relationship between the thermodynamic cloud properties A_c and τ and the optical properties R and ϵ within the context of a statistical cloud scheme. We restrict our attention to low clouds where the vertical profile of cloud liquid water is linear and where horizontal variability dominates. Assuming a known distribution of unresolved variability that includes cloud-top height fluctuations, we derive a self-consistent and computationally efficient set of equations for A_c and the moments of τ, thereby incorporating subgrid optical fluctuations into the statistical cloud schemes first introduced in the 1970s (Sommeria and Deardorff 1977; Mellor 1977). This unified treatment of thermodynamic and optical variability is particularly well suited for use in a GCM that incorporates a subgrid-scale turbulence scheme (Ricard and Royer 1993).

When cloud-top height fluctuations and temperature/moisture fluctuations are treated as a single random variable, then our model of longwave optical depth (liquid water path) reduces to the Considine et al. (1997) model if this new random variable is normally distributed. This approach, however, is not always valid. For example, a minimum large-scale lifting condensation level—breaking the reflection symmetry of cloud-base and cloud-

top height fluctuations—requires that cloud-base and cloud-top height fluctuations be treated distinctly (Jeffery and Davis 2002). Recent improvements in the retrieval of cloud physical properties using multiple remote sensors (Clothiaux et al. 2000; Wang and Sassen 2001) should provide more information on the joint statistics of cloud-base and cloud-top height fluctuations that could, in principle, be incorporated into our treatment of low-cloud optical depth.

Our unified approach can also be used to probe the sensitivity of parameterized cloud fraction and optical depth to changes in temperature. The coupled (ΔA_c, $\Delta\overline{\tau}$) global response of clouds to increasing temperature is analogous to the response of an open thermodynamic system. Although the particular thermodynamic trajectory that the system follows may be very sensitive to external forcing and boundary conditions, much can be learned by computing response functions where one of the thermodynamic coordinates is fixed along the trajectory. This approach was first considered by Temkin et al. (1975), who found $(\Delta A_c)_{\overline{\tau}} > 0$ and $(\Delta\overline{\tau})_{A_c} > 0$ using a nonstochastic model of a simplified atmosphere with one cloud layer and constant surface RH.

Using our statistical treatment of cloud optical variability, we derive analytic response functions in (A_c, $\overline{\tau}$, T) space that demonstrate the overall dominance of the cloud fraction feedback in the model. In contradistinction to Temkin et al. (1975), we find $(\Delta A_c)_{\overline{\tau}} < 0$. In particular, we show that the global observational evidence of a largely negative optical depth sensitivity presented by Tselioudis et al. (1993) produces in the model a much stronger negative cloud fraction response and therefore a net positive low cloud feedback. Also we find that low model vertical resolution can cause a significant overestimation of the unresolved low cloud A_c response by a factor of around 2.5. The accuracy of these results rests upon the crucial assumption that low-cloud A_c may be parameterized as a function of only relative humidity, an assumption that is typically made in large-scale models. Improvement in our understanding of the factors that control A_c at large scales is therefore a necessary next step towards the refinement in the formulation of the (A_c, $\overline{\tau}$) response functions introduced in this work.

Acknowledgments. We are grateful to Nicole Jeffery for a careful reading of the manuscript. We thank three anonymous reviewers for very thorough and constructive comments. This work was supported through funding of the Modeling of Clouds and Climate Proposal by the Canadian Foundation for Climate and Atmospheric Sciences, the Meteorological Service of Canada, and the Natural Sciences and Engineering Research Council.

APPENDIX A

Gaussian Relations for the h^2 Model

Recently Wood and Taylor (2001) derived

$$\sigma_{\mathrm{LWP}} \approx (2a_L\Gamma_w^{-1})^{1/2}\overline{\mathrm{LWP}}^{1/2}\sigma_s \qquad \text{(A1)}$$

using the h^2 model for LWP [see Eq. (5)], $z'_{\mathrm{top}} = 0$, Gaussian P_s, and assuming small σ_s/q_c where $q_c = q_t + \Gamma_w z_{\mathrm{top}} - q_0$. Wood and Taylor (2001) state Eq. (A1) is accurate to better than 5% for $\sigma_s/q_c < 1/2$. Below we present analytic expressions for $\overline{\mathrm{LWP}}$ and $\overline{\mathrm{LWP}^2}$, and hence σ_{LWP}, that are valid for all σ_s/q_c.

Using Eq. (5) and Gaussian P_{s*} we find

$$\overline{\mathrm{LWP}} = \frac{a_L}{2\Gamma_w}\left\{q_c^2 + \sigma_{s_*}^2 + \frac{q_c\sigma_{s_*}}{\sqrt{2\pi}}A_c^{-1}e^{-q_c^2/2\sigma_{s_*}^2}\right\}$$

$$\overline{\mathrm{LWP}^2} = \frac{a_L^2}{4\Gamma_w^2}\left\{q_c^4 + 6q_c^2\sigma_{s_*}^2 + 3\sigma_{s_*}^4 + \frac{A_c^{-1}}{\sqrt{2\pi}}(q_c^3\sigma_{s_*} + 5q_c\sigma_{s_*}^3)e^{-q_c^2/2\sigma_{s_*}^2}\right\}, \qquad \text{(A2)}$$

where $A_c = \mathrm{erfc}(-q_c/\sqrt{2}\sigma_{s*})/2$. Expanding (A2) to fourth order in small σ_{s*}/q_c gives

$$\sigma_{\mathrm{LWP}} \approx \left(\frac{2a_L}{\Gamma_w}\right)^{1/2}\sigma_{s_*}\left(\overline{\mathrm{LWP}} - \frac{a_L\sigma_{s_*}^2}{4\Gamma_w}\right)^{1/2},$$

from which (A1) follows approximately. Using Eq. (A2) we find that (A1) is accurate to better than 7% for $\sigma_{s*}/q_c < 1/2$.

A potential disadvantage of Eq. (A2) is that corresponding closed-form expressions for the $h^{5/3}$ model are not available; the modified triangle distribution introduced in appendix B has tractable noninteger moments and exhibits Gaussian behavior in close agreement with (A2).

APPENDIX B

Modified Triangle Distribution

Our modified triangle distribution is

$$P(s) = \frac{3}{2\sigma_0}\left(1 + \frac{5|s|}{3\sigma_0}\right)\left(1 - \frac{|s|}{\sigma_0}\right)^3, \quad -\sigma_0 \le s \le \sigma_0, \qquad \text{(B1)}$$

where $\sigma_0^2 = (35/3)\sigma_s^2$. Using Eqs. (1) and (B1), cloud fraction $A_c \equiv A_d(z_{\mathrm{top}})$ is

$$A_c = \begin{cases} 0 & Q_N \le -1 \\ (1 + Q_N)^4(1 - Q_N)/2 & -1 < Q_N \le 0 \\ 1 - (1 - Q_N)^4(1 + Q_N)/2 & 0 < Q_N < 1 \\ 1 & 1 \le Q_N, \end{cases}$$

where $Q_N = q_c/\sigma_0$ and $q_c = q_t + \Gamma_w z_{\mathrm{top}} - q_0$. The λ-th moment of the cloud liquid water used in the calculation of $\overline{\tau}$ via Eqs. (5) or (6) follows in a similar manner:

$$\overline{(q_c - s)^\lambda} = \begin{cases} 0 & Q_N \le -1 \\ A_c^{-1} F_1 & -1 < Q_N \le 0 \\ A_c^{-1}(F_1 + F_2) & 0 < Q_N < 1 \\ A_c^{-1}(F_1 + F_2 + F_3) & 1 \le Q_N, \end{cases}$$

where

$$F_1 = \frac{\sigma_0^\lambda (1 + Q_N)^{\lambda+4}}{2}\left\{\frac{3 - 5Q_N}{\lambda + 1} + \frac{-4 + 20Q_N}{\lambda + 2} + \frac{-6 - 30Q_N}{\lambda + 3} + \frac{12 + 20Q_N}{\lambda + 4} - \frac{5(1 + Q_N)}{\lambda + 5}\right\}$$

$$F_2 = \frac{\sigma_0^\lambda Q_N^{\lambda+1}}{16}\left\{\frac{-Q_N + 3Q_N^3}{\lambda + 1} + \frac{Q_N - 9Q_N^3}{\lambda + 2} + \frac{9Q_N^3}{\lambda + 3} - \frac{3Q_N^3}{\lambda + 4}\right\}$$

$$F_3 = \frac{\sigma_0^\lambda (-1 + Q_N)^{\lambda+4}}{2}\left\{\frac{3 + 5Q_N}{\lambda + 1} + \frac{-4 - 20Q_N}{\lambda + 2} + \frac{-6 + 30Q_N}{\lambda + 3} + \frac{12 - 20Q_N}{\lambda + 4} - \frac{5(1 - Q_N)}{\lambda + 5}\right\}.$$

APPENDIX C

Parameter Values

Parameter values are $q_0(T) = (1.826 \times 10^9 \text{ g m}^{-3}) \exp\{-R_v/(L_v T)\}$, $R_v = 461.5 \text{ J K}^{-1} \text{ kg}^{-1}$, $L_v = 2.5 \times 10^6 \text{ J kg}^{-1}$, $\Gamma_w = (4 \times 10^{-3} \text{ K m}^{-1}) \{L_v/(R_v T^2)\} q_0(T)$, $a_L = 0.75$, and the longwave absorption coefficient is $0.15 \text{ g}^{-1} \text{ m}^2$. The constant of proportionality in Eq. (6) is $2(k\pi)^{1/3} (4/3\rho_w)^{-2/3} N^{1/3}$ (Pontikis 1993) with parameter values $k = 1$, $\rho_w = 1 \text{ g cm}^{-3}$, and droplet number density $N = 200 \times 10^6 \text{ m}^{-3}$. The parameter k relates the effective and volume averaged radii. Parameter value $a_L = 0.75$ is consistent with a range of observations (e.g., Austin et al. 1995; Brenguier et al. 2000).

APPENDIX D

LCF Parameter Values

Shortwave cloud forcing: no absorption, surface albedo is from Robock (1980), $\partial \ln\overline{\tau}/\partial T = 0.01 - 0.14 \exp(-0.00175\phi^2) \text{ K}^{-1}$ is parameterized from Tselioudis et al. (1993), and the solar constant is 1365 W m^{-2}. Longwave cloud forcing: water vapor forcing is ignored and cloud-top temperature is $T + 6.5$°C.

REFERENCES

Albrecht, B. A., C. W. Fairall, D. W. Thomson, and A. B. White, 1990: Surface-based remote sensing of the observed and the adiabatic liquid water content of stratocumulus clouds. *Geophys. Res. Lett.,* **17,** 89–92.

Arking, A., 1991: The radiative effects of clouds and their impact on climate. *Bull. Amer. Meteor. Soc.,* **72,** 795–813.

Austin, P., Y. Wang, R. Pincus, and V. Kujala, 1995: Precipitation in stratocumulus clouds: Observational and modeling results. *J. Atmos. Sci.,* **52,** 2329–2352.

Bajuk, L. J., and C. B. Leovy, 1998: Seasonal and interannual variations in stratiform and convective clouds over the tropical Pacific and Indian Oceans from ship observations. *J. Climate,* **11,** 2922–2941.

Barker, H. W., 1996: A parameterization for computing grid-averaged solar fluxes for inhomogeneous marine boundary layer clouds. Part I: Methodology and homogeneous biases. *J. Atmos. Sci.,* **53,** 2289–2303.

——, and B. A. Wielicki, 1997: Parameterizing grid-averaged longwave fluxes for inhomogeneous marine boundary layer clouds. *J. Atmos. Sci.,* **54,** 2785–2798.

——, ——, and L. Parker, 1996: A parameterization for computing grid-averaged solar fluxes for inhomogeneous marine boundary layer clouds. Part II: Validation using satellite data. *J. Atmos. Sci.,* **53,** 2304–2316.

Boers, R., J. D. Spinhirne, and W. D. Hart, 1988: Lidar observations of the fine-scale variability of marine stratocumulus clouds. *J. Appl. Meteor.,* **27,** 797–810.

Bony, S., K.-M. Lau, and Y. C. Sud, 1997: Sea surface temperature and large-scale circulation influences on tropical greenhouse effect and cloud radiative forcing. *J. Climate,* **10,** 2055–2077.

Brenguier, J.-L., H. Pawlowska, L. Schüller, R. Preusker, J. Fischer, and Y. Fouquart, 2000: Radiative properties of boundary layer clouds: Droplet effective radius versus number concentration. *J. Atmos. Sci.,* **57,** 803–821.

Browning, K. A., 1994: Survey of perceived priority issues in the parameterizations of cloud-related processes in GCMs. *Quart. J. Roy. Meteor. Soc.,* **120,** 483–487.

Bushell, A. C., and G. M. Martin, 1999: The impact of vertical resolution upon GCM simulations of marine stratocumulus. *Climate Dyn.,* **15,** 293–318.

Cahalan, R. F., W. Ridgway, W. J. Wiscombe, T. L. Bell, and J. B. Snider, 1994: The albedo of fractal stratocumulus clouds. *J. Atmos. Sci.,* **51,** 2434–2455.

Cess, R. D., G. L. Potter, and J. P. Blanchet, 1990: Intercomparison and interpretation of climate feedback processes in 19 atmospheric general circulation models. *J. Geophys. Res.,* **95** (D10), 16 601–16 615.

Chen, T., W. B. Rossow, and Y. Zhang, 2000: Radiative effects of cloud-type variations. *J. Climate,* **13,** 264–286.

Clothiaux, E. E., T. P. Ackerman, G. G. Mace, K. P. Moran, R. T. Marchand, M. A. Miller, and B. E. Martner, 2000: Objective determination of cloud heights and radar reflectivities using a combination of active remote sensors at the ARM CART sites. *J. Appl. Meteor.,* **39,** 645–665.

Colman, R. A., and B. J. McAvaney, 1997: A study of general circulation model climate feedbacks determined from perturbed sea surface temperature experiments. *J. Geophys. Res.,* **102** (D16), 19 383–19 402.

Considine, G., J. A. Curry, and B. Wielicki, 1997: Modeling cloud fraction and horizontal variability in marine boundary layer clouds. *J. Geophys. Res.,* **102** (D12), 13 517–13 525.

Cuijpers, J. W. M., and P. Bechtold, 1995: A simple parameterization of cloud water related variables for use in boundary layer models. *J. Atmos. Sci.,* **52,** 2486–2490.

Cusack, S., J. M. Edwards, and R. Kershaw, 1999: Estimating the subgrid variance of saturation, and its parameterization for use in a GCM cloud scheme. *Quart. J. Roy. Meteor. Soc.,* **125,** 3057–3076.

Deardorff, J. W., 1974: Three-dimensional numerical study of turbulence in an entraining mixed layer. *Bound.-Layer Meteor.,* **7,** 199–226.

——, 1981: On the distribution of mean radiative cooling at the top of a stratocumulus-capped mixed layer. *Quart. J. Roy. Meteor. Soc.,* **107,** 191–202.

Greenwald, T. J., G. L. Stephens, S. A. Christopher, and T. H. Vonder Haar, 1995: Observations of the global characteristics and regional radiative effects of marine cloud liquid water. *J. Climate,* **8,** 2928–2946.

Hansen, J., A. Lacis, D. Rind, and G. Russell, 1984: Climate sensitivity: Analysis of feedback mechanisms. *Climate Processes and Climate Sensitivity, Geophys. Monogr.,* No. 29, Amer. Geophys. Union, 130–163.

Hatzianastassiou, N., and I. Vardavas, 1999: Shortwave radiation budget of the northern hemisphere using International Satellite Cloud Climatology Project and NCEP/NCAR climatological data. *J. Geophys. Res.,* **104** (D20), 24 401–24 421.

Jeffery, C. A., 2001: Statistical models of cloud-turbulence interactions. Ph.D. thesis, University of British Columbia, Vancouver, Canada, 122 pp.

——, and A. B. Davis, 2002: Signature of cloud-base-height skewness in ARM microwave water radiometer data: Implications for cloud radiative parameterizations in GCMs. *Proc. SPIE,* **4815,** 9–19.

Klein, S. A., and D. L. Hartmann, 1993: The seasonal cycle of low stratiform clouds. *J. Climate,* **6,** 1587–1606.

——, ——, and J. R. Norris, 1995: On the relationships among low-cloud structure, sea surface temperature, and atmospheric circulation in the summertime northeast Pacific. *J. Climate,* **8,** 1140–1155.

Kogan, Z. N., Y. L. Kogan, and D. L. Lilly, 1997: Cloud factor and seasonality of the indirect effect of anthropogenic sulfate aerosols. *J. Geophys. Res.,* **102** (D22), 25 927–25 939.

Larson, V. E., R. Wood, P. R. Field, J.-C. Golaz, T. H. Vonder Haar, and W. R. Cotton, 2001: Small-scale and mesoscale variability of scalars in cloudy boundary layers: One-dimensional probability density functions. *J. Atmos. Sci.,* **58,** 1978–1994.

Levkov, L., B. Rockel, H. Schiller, and L. Kornblueh, 1998: 3-D simulation of clouds with subgrid fluctuations of temperature and humidity. *Atmos. Res.,* **47–48,** 327–341.

Loeb, N. G., T. Várnai, and D. M. Winker, 1998: Influence of subpixel-scale cloud-top structure on reflectances from overcast stratiform cloud layers. *J. Atmos. Sci.,* **55,** 2960–2973.

Manabe, S., and R. T. Wetherald, 1967: Thermal equilibrium of the atmosphere with a given distribution of relative humidity. *J. Atmos. Sci.,* **24,** 241–259.

——, and R. J. Stouffer, 1979: A CO_2-climate sensitivity study with a mathematical model of the global climate. *Nature,* **282,** 491–493.

Mellor, G. L., 1977: The Gaussian cloud model relations. *J. Atmos. Sci.,* **34,** 356–358; Corrigendum, **34,** 1483.

Moeng, C. H., P. P. Sullivan, and B. Stevens, 1999: Including radiative effects in an entrainment rate formula for buoyancy-driven PBLs. *J. Atmos. Sci.,* **56,** 1031–1049.

Norris, J. R., 1998a: Low cloud type over the ocean from surface observations. Part I: Relationship to surface meteorology and the vertical distribution of temperature and moisture. *J. Climate,* **11,** 369–382.

——, 1998b: Low cloud type over the ocean from surface observations. Part II: Geographical and seasonal variations. *J. Climate,* **11,** 383–403.

——, and C. B. Leovy, 1994: Interannual variability in stratiform cloudiness and sea surface temperature. *J. Climate,* **7,** 1915–1925.

Oreopoulos, L., and R. Davies, 1993: Statistical dependence of albedo and cloud cover on sea surface temperature for two tropical marine stratocumulus regions. *J. Climate,* **6,** 2434–2447.

Pincus, R., and S. A. Klein, 2000: Unresolved spatial variability and microphysical process rates in large-scale models. *J. Geophys. Res.,* **105** (D22), 27 059–27 065.

Pontikis, C., 1993: Parameterization of the cloud optical thickness: Influence of clear air entrainment. *Geophys. Res. Lett.,* **20,** 2655–2658.

Ramaswamy, V., and C.-T. Chen, 1993: An investigation of the global solar radiative forcing due to changes in cloud liquid water path. *J. Geophys. Res.,* **98** (D9), 16 703–16 712.

Ricard, J. L., and J. F. Royer, 1993: A statistical cloud scheme for use in an AGCM. *Ann. Geophys.,* **11,** 1095–1115.

Robock, A., 1980: The seasonal cycle of snow cover, sea ice and surface albedo. *Mon. Wea. Rev.,* **108,** 267–285.

Rotstayn, L. D., 1997: A physically based scheme for the treatment of stratiform clouds and precipitation in large-scale models. I: Description and evaluation of the microphysical processes. *Quart. J. Roy. Meteor. Soc.,* **123,** 1227–1282.

——, 1999: Climate sensitivity of the CSIRO GCM: Effects of cloud modeling assumptions. *J. Climate,* **12,** 334–356.

Schneider, S. H., W. M. Washington, and R. M. Chervin, 1978: Cloudiness as a climatic feedback mechanism: Effects on cloud amounts of prescribed global and regional surface temperature changes in the NCAR GCM. *J. Atmos. Sci.,* **35,** 2207–2221.

Smith, R. N. B., 1990: A scheme for predicting layer clouds and their water content in a general circulation model. *Quart. J. Roy. Meteor. Soc.,* **116,** 435–460.

Somerville, R. C. J., and L. A. Remer, 1984: Cloud optical thickness feedbacks in the CO_2 climate problem. *J. Geophys. Res.,* **89** (D6), 9668–9672.

Sommeria, G., and J. W. Deardorff, 1977: Subgrid-scale condensation in models of nonprecipitating clouds. *J. Atmos. Sci.,* **34,** 344–355.

Strawbridge, K. B., and R. M. Hoff, 1996: LITE validation experiment along California's coast: Preliminary results. *Geophys. Res. Lett.,* **23,** 73–76.

Temkin, R. L., B. C. Weare, and F. M. Snell, 1975: Feedback coupling of absorbed solar radiation by three model atmospheres with clouds. *J. Atmos. Sci.,* **32,** 873–880.

Tselioudis, G., A. A. Lacis, D. Rind, and W. B. Rossow, 1993: Potential effects of cloud optical thickness on climate warming. *Nature,* **366,** 670–672.

——, A. D. Del Genio, W. Kovari, and M.-S. Yao, 1998: Temperature dependence of low cloud optical thickness in the GISS GCM: Contributing mechanisms and climate implications. *J. Climate,* **11,** 3268–3281.

Wang, Z., and K. Sassen, 2001: Cloud type and macrophysical property retrieval using multiple remote sensors. *J. Appl. Meteor.,* **40,** 1665–1682.

Warren, S. G., C. J. Hahn, J. London, R. M. Chervin, and R. L. Jenne, 1988: Global distribution of total cloud cover and cloud type amounts over the ocean. Tech. Note TN-317+STR, NCAR, Boulder, CO, 305 pp.

Wetherald, R. T., and S. Manabe, 1986: An investigation of cloud cover change in response to thermal forcing. *Climatic Change,* **8,** 5–23.

Wood, R., and J. P. Taylor, 2001: Liquid water path variability in unbroken marine stratocumulus cloud. *Quart. J. Roy. Meteor. Soc.,* **127,** 2635–2662.

Xu, K.-M., and D. A. Randall, 1996: Evaluation of statistically based cloudiness parameterizations used in climate models. *J. Atmos. Sci.,* **53,** 3103–3119.

Yao, M.-S., and A. D. Del Genio, 1999: Effects of cloud parameterization on the simulation of climate changes in the GISS GCM. *J. Climate,* **12,** 761–779.